

## Strongly capacitively coupled quantum dots

I. H. Chan and R. M. Westervelt<sup>a)</sup>

*Division of Engineering and Applied Sciences and Department of Physics, Harvard University, Cambridge, Massachusetts 02138*

K. D. Maranowski<sup>b)</sup> and A. C. Gossard

*Materials Department and Department of Electrical and Computer Engineering, University of California, Santa Barbara, California 93106*

(Received 18 September 2001; accepted for publication 20 December 2001)

Double quantum dots were formed in a gated GaAs/AlGaAs heterostructure with negligible interdot tunneling; strong capacitive coupling was provided by a floating interdot capacitor. The interdot capacitance was measured to be  $0.28C_{\Sigma}$ , where  $C_{\Sigma}$  is the single-dot capacitance. Coulomb blockade conductance images for both dots versus side gate voltages at 70 mK show a hexagonal pattern of peaks; the double dot acts as a single-electron current switch. For weak tunneling, the conductance peaks of both dots fit thermally broadened line shapes. Charge fluctuations produced by strong tunneling on one dot are induced on the second, filling in its peak splitting. © 2002 American Institute of Physics. [DOI: 10.1063/1.1456552]

Quantum dots show a range of important phenomena including the Coulomb blockade, single-electron transport, and individual electronic states.<sup>1–3</sup> Circuits of quantum dots are being studied now to provide approaches to sensors and electronics. Coupling dots together via electron tunneling mimics molecular bonds formed between atoms.<sup>4–9</sup> Tunnel-coupled quantum dots have opened avenues of study, including proposed implementations of quantum information processing.<sup>10</sup> Coupling two or more quantum dots via interdot capacitors provides an additional way to correlate electrons and build circuits for logic and quantum information processing.

In this letter, we describe the use of an interdot capacitor to form a strongly coupled double quantum dot with no interdot tunneling. In conventional laterally defined double quantum dots formed from a two-dimensional electron gas (2DEG) in a GaAs/AlGaAs heterostructure, the edge-on capacitance between dots is small, and an excess electron on one dot only has a linear effect on the conductance of the adjacent dot.<sup>11</sup> In the present work, capacitor plates were added over each dot to increase the interdot capacitance significantly. Because the interdot capacitor is electrically floating and comparable in size to the dots, it can rapidly transfer small induced charges from one dot to the other. In Coulomb blockade measurements at He dilution refrigerator temperatures, a single excess electron on one dot switched the other dot on or off its Coulomb blockade peak, changing its electrical conductance by two decades. In addition, charge fluctuations caused by lifetime broadening in one dot are induced on the second dot kept in the weak tunneling regime. The conductance peaks of the two dots fit a combination of thermally broadened and lifetime broadened line shapes.

A scanning electron microscope image of the double-dot device used in this experiment is shown in Fig. 1(a) with a schematic diagram in Fig. 1(b). The two quantum dots were formed in a 2DEG inside a GaAs/AlGaAs heterostructure

with the following layers (surface down): 50 Å GaAs, 300 Å  $\text{Al}_{0.3}\text{Ga}_{0.7}\text{As}$ ,  $8 \times 10^{12} \text{ cm}^{-2}$  Si  $\delta$ -doping layer, 220 Å  $\text{Al}_{0.3}\text{Ga}_{0.7}\text{As}$ , and 10 000 Å GaAs on a GaAs substrate. The 2DEG has mobility  $\mu = 5 \times 10^5 \text{ cm}^2/\text{Vs}$  and density  $n_s = 3 \times 10^{11} \text{ cm}^{-2}$  at liquid-He temperatures. The two rectangular quantum dots shown in Fig. 1(a) are defined on three sides by Cr–Au gates (light regions) and on the fourth side by a 50-nm-deep trench (very dark region) down the center of the device. A special feature of this device is the floating interdot capacitor that consists of two capacitor plates, one over each dot, connected by a thick bridge of Cr–Au (very light center bar). The trench down the center of the device prevents tunneling between the two dots ( $R \gg 10 \text{ M}\Omega$ ), so that interactions between the dots arise from capacitive coupling and not tunneling. Both dots are nominally identical with lithographic dimensions  $500 \times 800 \text{ nm}^2$ . The left-hand dot will be referred to as dot 1 and the right hand dot as dot 2; their respective side gate voltages are  $V_{G1}$  and  $V_{G2}$ . Electrical measurements of the device were made in a He dilution refrigerator held at the base temperature 10 mK. The measured electron temperature 70 mK was determined from the widths of the Coulomb blockade conductance peaks. Two leads were connected to each dot by quantum point contacts. The conductances  $G_{D1}$  and  $G_{D2}$  of the two dots were measured simultaneously using two lock-in amplifiers at different frequencies.

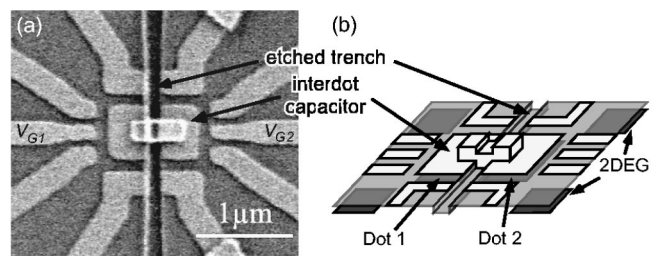


FIG. 1. (a) Scanning electron micrograph of a capacitively coupled double quantum dot formed in a GaAs/AlGaAs heterostructure. Light areas are metal gates; the dark vertical trench prevents tunneling between dots; the bright bar in the center connects two capacitor plates above each dot, forming an interdot capacitor. (b) Schematic diagram of the device.

<sup>a)</sup>Electronic mail: westervelt@deas.harvard.edu

<sup>b)</sup>Current address: Cielo Communications, 325 Interlocken Parkway, Bldg. A, Broomfield, CO 80021.

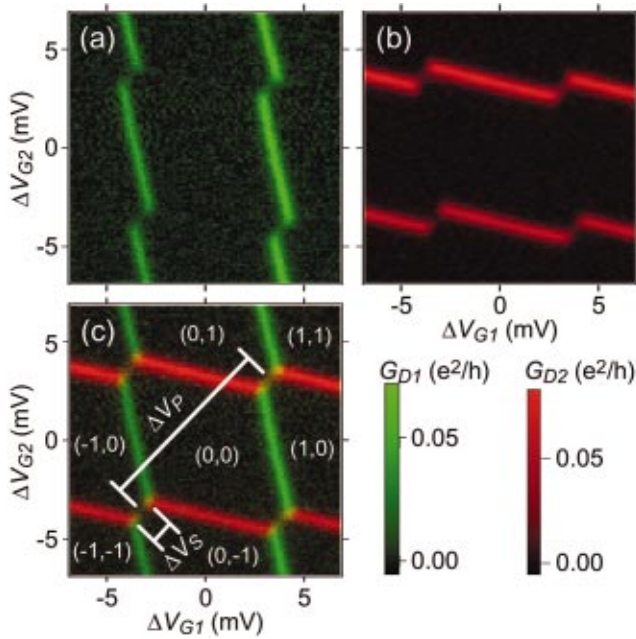


FIG. 2. (Color) Coulomb blockade conductance (a)  $G_{D1}$  for dot 1 and (b)  $G_{D2}$  for dot 2 vs side gate voltages  $\Delta V_{G1}$  and  $\Delta V_{G2}$ . The light areas are Coulomb blockade peaks which split abruptly as electrons are added or removed from the adjacent dot. (c) Superposition of data in (a) and (b) showing peak splitting  $\Delta V_S$  and period  $\Delta V_P$ .

Figures 2(a) and 2(b) show images of conductances  $G_{D1}$  and  $G_{D2}$ , respectively, versus changes in side gate voltages  $\Delta V_{G1}$  and  $\Delta V_{G2}$  of the two dots. The bright regions have high conductance and the dark regions have low conductance and fixed dot charge. For these measurements, the tunnel barriers to both dots were set in the weak-tunneling regime ( $G \ll 2e^2/h$ ), so that the number of electrons on each dot ( $\sim 800$ ) was well defined and the Coulomb blockade conductance peaks were thermally broadened. The pattern of lines in Fig. 2(a) is not seen in Fig. 2(b) and vice versa, because no tunneling occurs between the dots. The key feature of these images is the systematic and reproducible presence of splits in the Coulomb blockade peak for each dot due to the addition or removal of one electron from the adjacent dot. Figure 2(c) is a superposition of Figs. 2(a) and 2(b); the splits in both dots occur at the same gate voltage changes  $\Delta V_{G1}$  and  $\Delta V_{G2}$ , where the Coulomb blockade peaks of both dots are suppressed.

As shown in Fig. 2(c), conductances  $G_{D1}$  and  $G_{D2}$  form a hexagonal pattern very similar to the Coulomb blockade pattern observed for a tunnel-coupled double dot.<sup>4</sup> The individual hexagons in Fig. 2(c) are labeled by the number of electrons ( $n_1, n_2$ ) in dots 1 and 2, respectively. The electrostatic energy of the double dot is a minimum at the center of each hexagon. Moving in the direction  $\Delta V_{G1} = \Delta V_{G2}$  increases the total double-dot charge in steps of  $2e$  between hexagons. Changing the gate voltages in the perpendicular direction  $\Delta V_{G1} = -\Delta V_{G2}$  keeps the total charge constant, but increases the double-dot polarization by transferring one electron from dot 1 to dot 2. Coulomb blockade peaks are suppressed in the splits, because the electron numbers  $n_1$  and  $n_2$  must change simultaneously for conduction to occur.

The interdot capacitance  $C_{INT}$  is determined by<sup>12</sup> the ratio of peak splitting  $\Delta V_S$  and period  $\Delta V_P$  indicated in Fig.

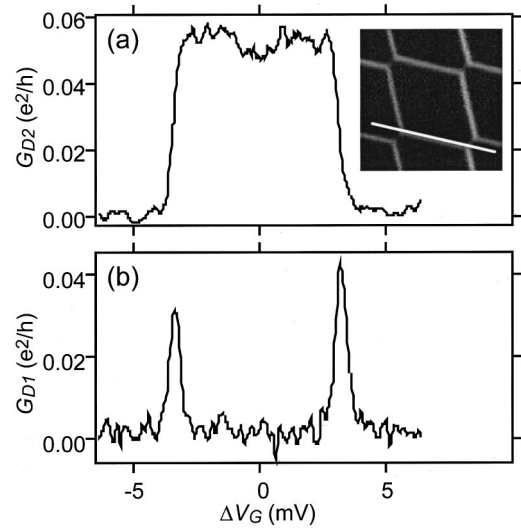


FIG. 3. Conductance (a)  $G_{D2}$  for dot 2 and (b)  $G_{D1}$  for dot 1 along the white line path in the inset. The addition of one electron to dot 1 switches dot 2 on or off a Coulomb blockade peak.

2(c) and the total capacitance of each dot to ground  $C_\Sigma$ :

$$C_{INT} = \frac{2\Delta V_S}{\Delta V_P} C_\Sigma. \quad (1)$$

Substituting the measured ratio  $\Delta V_S/\Delta V_P = 0.14 \pm 0.01$  and  $C_\Sigma = 530 \pm 30$  aF (from finite voltage bias Coulomb blockade measurements) into Eq. (1), we obtain  $C_{INT} = 0.28C_\Sigma = 150 \pm 20$  aF. This interdot capacitance is considerably larger than the values  $C_{INT} = 0.03C_\Sigma$  and  $C_{INT} = 0.05C_\Sigma$  reported for planar double dots of similar shapes without interdot capacitors.<sup>4,5</sup>

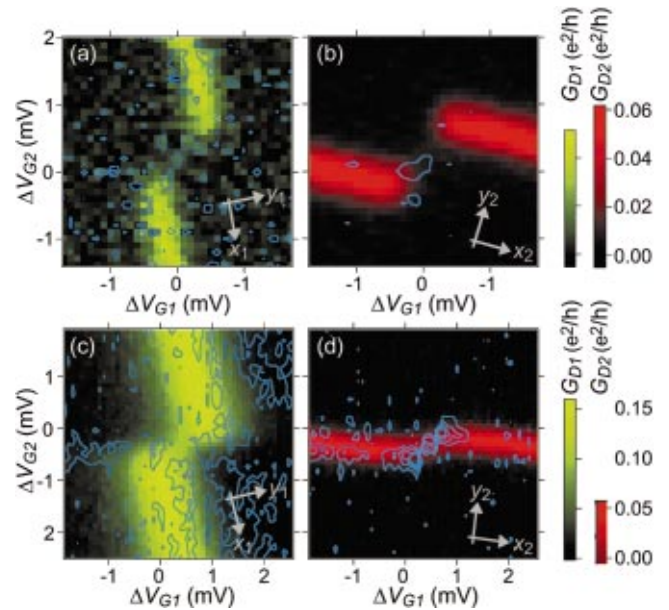


FIG. 4. (Color) Conductance near the peak split (a), (c)  $G_{D1}$  for dot 1 and (b), (d)  $G_{D2}$  for dot 2, overlaid with contours showing the error to line-shape fits, and with axes used in those fits. Contour separation is  $0.0075 e^2/h$  for dot 1 and  $0.005 e^2/h$  for dot 2; contours of zero error are not shown. (a) and (b) images of  $G_{D1}$  and  $G_{D2}$  with both dots in the weak-tunneling regime. Thermally broadened line shapes fit the data for both dots. (c) and (d) images of  $G_{D1}$  and  $G_{D2}$  with dot 1 in the strong-tunneling regime and dot 2 in the weak-tunneling regime. Combined finite lifetime line-shape and thermally broadened line-shape fits agree with the data.

The practical consequence of strong interdot coupling is that an additional electron in one dot can bias the other dot completely on or off a Coulomb blockade peak to form a switch. Figures 3(a) and 3(b) show  $G_{D2}$  and  $G_{D1}$  for gate voltage changes along the white line path in the inset. When an electron is added to dot 1 at  $\Delta V_G \approx -3$  mV, the conductance of dot 2 is switched onto a conductance peak from the blocked regime, increasing  $G_{D2}$  by about two orders of magnitude. When an additional electron enters dot 1 at  $\Delta V_G \approx +3$  mV, it moves dot 2 off the conductance peak into the blocked regime, switching the current in dot 2 off. Peak splitting  $\Delta V_S$  in Fig. 2(c) corresponds to an energy shift of  $8 k_B T_e$  at electron temperature  $T_e = 70$  mK, making this switch tolerant against thermal fluctuations.

Figures 4(a) to 4(d) show close-up images of  $G_{D1}$  and  $G_{D2}$  near the conductance peak splits. Overlaid on top are contour lines showing the error in fits of theory to the Coulomb blockade conductance ridges; the axes used in each fit are indicated. The top two images in Figs. 4(a) and 4(b) for dots 1 and 2, respectively, were acquired when both dots were in the weak-tunneling regime. For these conditions, we used thermally broadened line shapes to fit the Coulomb blockade conductance ridges  $G_{D1}(x_1, y_1)$  in Fig. 4(a) and  $G_{D2}(x_2, y_2)$  in Fig. 4(b):

$$G_{D1}(x_1, y_1) = G_0 + G_{\max} \left( \frac{1 + \tanh[A(x_1 - x_0)]}{2 \cosh^2[A(y_1 - y_0)]} + \frac{1 + \tanh[A(x_0 - x_1)]}{2 \cosh^2[A(y_0 - y_1)]} \right), \quad (2a)$$

$$G_{D2}(x_2, y_2) = G_0 + G_{\max} \left( \frac{1 + \tanh[A(x_2 - x_0)]}{2 \cosh^2[A(y_2 - y_0)]} + \frac{1 + \tanh[A(x_0 - x_2)]}{2 \cosh^2[A(y_0 - y_2)]} \right). \quad (2b)$$

For Fig. 4(a), the axis  $x_1$  corresponds to constant induced charge on dot 1; it is perpendicular to axis  $y_1$ . Locations  $(x_0, y_0)$  and  $(x_{00}, y_{00})$  in the gate voltage correspond to the ends of the two conductance ridges on opposite sides of the split. They are adjusted in the fit along with parameters  $G_0$ ,  $G_{\max}$ , and  $A$ . The variables describing conductance  $G_{D2}(x_2, y_2)$  of dot 2 in Fig. 4(b) have similar definitions. The  $\cosh^{-2}(y)$  terms in Eqs. (2a) and (2b) are the standard line shapes for thermal broadening. The  $[1 + \tanh(x)]/2$  terms represent thermally broadened step functions obtained by integrating the thermal line shapes along the  $x$  axes. Equations (2a) and (2b) fit the conductance data in Figs. 4(a) and 4(b) very well, as indicated by the residual contours. A small connecting feature linking the ends of the conductance ridges is discernible in the error due to the slight additional conductance where hexagons  $(n_1 + 1, n_2)$  and  $(n_1, n_2 + 1)$  meet.

The bottom two images in Figs. 4(c) and 4(d) were acquired with dot 1 in the strong-tunneling regime and dot 2 in the weak-tunneling regime. It is clear from Fig. 4(c) that the conductance ridges of dot 1 are much broader than for weak tunneling, but even more interesting are the sharp, rectangular terminations of the conductance ridges at the split. Dot 2 is in the weak-tunneling regime, and its charge is well quantized, so the peak splitting for dot 1 remains sharp. On the other hand, the width of the conductance ridges for dot 2 are

narrow, but the peak splitting for dot 2 is partially filled in, because the charge on dot 1 is not well quantized. Fits to the conductance ridges in Figs. 4(c) and 4(d) were made to a lifetime broadened line shape along one axis [ $y_1$  for Fig. 4(c) and  $x_2$  for Fig. 4(d)] and to a thermally broadened line shape along the perpendicular axis. Using a Lorentzian line shape for lifetime broadening, expressions  $G_{D1}(x_1, y_1)$  for dot 1 in Fig. 4(c) and  $G_{D2}(x_2, y_2)$  for dot 2 in Fig. 4(d) are

$$G_{D1}(x_1, y_1) = G_0 + G_{\max} \left( \frac{1 + \tanh[A(x_1 - x_0)]}{2 + 2[B(y_1 - y_0)]^2} + \frac{1 + \tanh[A(x_0 - x_1)]}{2 + 2[B(y_0 - y_1)]^2} \right), \quad (3a)$$

$$G_{D2}(x_2, y_2) = G_0 + G_{\max} \left( \frac{\pi/2 + \arctan[A(x_2 - x_0)]}{\pi \cosh^2[B(y_2 - y_0)]} + \frac{\pi/2 + \arctan[A(x_0 - x_2)]}{\pi \cosh^2[B(y_0 - y_2)]} \right). \quad (3b)$$

The definition of the terms used in Eqs. (3a) and (3b) are the same as in Eqs. (2a) and (2b), with the addition of a new parameter  $B$ . The terms  $[\pi/2 + \arctan(x_2)]/\pi$  in Eq. (3b) represent lifetime broadened step functions obtained by integrating the lifetime broadened line shape along the  $x_2$  axis. Equation (3a) fits the data in Fig. 4(c) well, because the peak split is clearly defined. Equation (3b) fits the data in Fig. 4(d) well except for an interesting feature where the partial loss of charge quantization in dot 1 bends the conductance ridges of dot 2 at the split.

The authors thank D. Goldhaber-Gordon and L. Kouwenhoven for useful comments. This work was supported at Harvard University by NSF Grant No. DMR-98-0-2242, DARPA Grant No. DAAD19-01-1-0659, ONR Grant No. N00014-99-1-0347, and MRSEC NSF Grant No. DMR-98-09363, and at the University of California, Santa Barbara by the QUEST NSF Science and Technology Center.

<sup>1</sup>H. Grabert and M. H. Devoret, NATO ASI Ser., Ser. B **294**, (1992), and references contained therein.

<sup>2</sup>L. L. Sohn, L. P. Kouwenhoven, and G. Schön, NATO ASI Ser., Ser. E **345**, (1997), and references contained therein.

<sup>3</sup>K. K. Likharev, Proc. IEEE **87**, 606 (1999), and references contained therein.

<sup>4</sup>C. Livermore, C. H. Crouch, R. M. Westervelt, K. L. Campman, and A. C. Gossard, Science **274**, 1332 (1996).

<sup>5</sup>N. C. van der Vaart, S. F. Godijn, Y. V. Nazarov, C. J. P. M. Harmans, J. E. Mooij, L. W. Molenkamp, and C. T. Foxon, Phys. Rev. Lett. **74**, 4702 (1995).

<sup>6</sup>F. R. Waugh, M. J. Berry, D. J. Mar, R. M. Westervelt, K. L. Campman, and A. C. Gossard, Phys. Rev. Lett. **75**, 705 (1995).

<sup>7</sup>F. Hofmann, T. Heinzl, D. A. Wharam, J. P. Kotthaus, G. Böhm, W. Klein, G. Tränkle, and G. Weimann, Phys. Rev. B **51**, 13 872 (1995).

<sup>8</sup>R. H. Blick, R. J. Haug, J. Weiss, D. Pfannkuche, K. v. Klitzing, and K. Eberl, Phys. Rev. B **53**, 7899 (1996).

<sup>9</sup>D. Dixon, L. P. Kouwenhoven, P. L. McEuen, Y. Nagamune, J. Motohisa, and N. Sakaki, Phys. Rev. B **53**, 12 625 (1996).

<sup>10</sup>D. Loss and D. P. DiVincenzo, Phys. Rev. A **57**, 120 (1998).

<sup>11</sup>D. S. Duncan, C. Livermore, R. M. Westervelt, K. D. Maranowski, and A. C. Gossard, Appl. Phys. Lett. **74**, 1045 (1999)

<sup>12</sup>C. Livermore, D. S. Duncan, R. M. Westervelt, K. D. Maranowski, and A. C. Gossard, J. Appl. Phys. **86**, 4043 (1999).